Succinate metabolism in the retinal pigment epithelium uncouples respiration from ATP synthesis

Daniel T. Hass[1], **Celia M. Bisbach**[1,2], **Brian M. Robbings**[1,3], **Martin Sadilek**[4], **Ian R. Sweet**[3,5], **James B. Hurley**[1,6,7,*]

[1]Biochemistry Department, The University of Washington, Seattle, WA 98195, USA

[2]Promega Corporation, 2800 Woods Hollow Road, Fitchburg, WI 53711, USA

[3]Diabetes Institute, The University of Washington, Seattle, WA 98109, USA

[4]Chemistry Department, The University of Washington, Seattle, WA 98195, USA

[5]Division of Metabolism, Endocrinology and Nutrition, The University of Washington, Seattle, WA 98195, USA

[6]Opthalmology Department, The University of Washington, Seattle, WA 98109, USA

[7]Lead contact

SUMMARY

Fumarate can be a surrogate for O_2 as a terminal electron acceptor in the electron transport chain. Reduction of fumarate produces succinate, which can be exported. It is debated whether intact tissues can import and oxidize succinate produced by other tissues. In a previous report, we showed that mitochondria in retinal pigment epithelium (RPE)-choroid preparations can use succinate to reduce O_2 to H_2O. However, cells in that preparation could have been disrupted during tissue isolation. We now use multiple strategies to quantify intactness of the isolated RPE-choroid tissue. We find that exogenous $^{13}C_4$-succinate is oxidized by intact cells then exported as fumarate or malate. Unexpectedly, we also find that oxidation of succinate is different from oxidation of other substrates because it uncouples electron transport from ATP synthesis. Retinas produce and export succinate. Our findings imply that retina succinate may substantially increase O_2 consumption by uncoupling adjacent RPE mitochondria.

Graphical Abstract

In brief

The retina releases succinate, a source of reducing power for mitochondria. Hass et al. outline a pathway by which retina succinate can enter intact RPE-choroid cells and stimulate mitochondrial respiration that is uncoupled from ATP synthesis. Rapid RPE succinate oxidation may limit O_2 levels in the retina.

INTRODUCTION

Mitochondria are the principal sites of cellular O_2 consumption. O_2 consumption rate (OCR) depends on partial O_2 pressure (pO_2) and substrate levels. Mammalian tissues normally operate at a $pO_2 < 70$ mm Hg (Ast and Mootha, 2019; Keeley and Mann, 2019). In the photoreceptor layer of mammalian retinas, the physiological pO_2 is far lower at $pO_2 < 15$ mm Hg (Linsenmeier and Zhang, 2017; Yu and Cringle, 2006).

When pO_2 is low, it can affect electron transport in mitochondria by diverting electrons to reduce fumarate to succinate rather than reducing O_2 to H_2O (Bisbach et al., 2020; Chouchani et al., 2014; Spinelli et al., 2021). Reduction of fumarate to succinate occurs in hypoxic tissues, and it is generally considered a deviation from normal tricarboxylic acid (TCA) cycle metabolism (Chouchani et al., 2014; Hochachka et al., 1975).

Recent findings suggest that reduction of fumarate to succinate may be normal for some tissues in physiological settings where pO_2 is low (Spinelli et al., 2021; Bisbach et al., 2020). For example, retinas produce and export succinate (Bisbach et al., 2020), and exercising muscle depleted of O_2 generates succinate and releases it into circulation (Hochachka and Dressendorfer, 1976; Mills et al., 2021).

Circulating succinate can affect metabolism in downstream tissues. Succinate can stimulate brown adipose tissue thermogenesis (Mills et al., 2018, 2021). Succinate also can stimulate consumption of O_2 by retinal pigment epithelium (RPE) tissue isolated from mouse eyes (Bisbach et al., 2020). However, some reports have suggested that intact cells do not metabolize succinate and that oxidation of succinate occurs only when cells within the tissue have been permeabilized (Jolly et al., 1979; Ehinger et al., 2016; MacDonald et al., 1989).

In this report we rigorously address the hypothesis that intact RPE-choroid imports and oxidizes succinate. We use multiple independent strategies to address the possibility that oxidation of succinate in these preparations occurs only in broken cells. We find that most of the succinate metabolized by RPE-choroid preparations is oxidized by mitochondria within intact cells. We were surprised to find that succinate utilization also stimulates uncoupling of mitochondrial electron transport from ATP synthesis. The retina is one of many tissues that release succinate (Jang et al., 2019; Reddy et al., 2020; Bisbach et al., 2020). Our findings show that in physiological settings where succinate release is favorable, succinate released from one tissue may fuel metabolism and uncouple mitochondria in another tissue.

RESULTS

Tissue preparation

To evaluate the ability of RPE cells to import and oxidize succinate, we use a mouse RPE-choroid preparation. To prepare RPE-choroid, we euthanize each mouse, enucleate its eye, and trim away extraocular muscles. We cut at the ora serrata, removing the lens, then the retina. We place the remaining RPE-choroid in culture medium. The outer surface of this preparation is metabolically inactive scleral connective tissue. The inner surface is a monolayer of metabolically active RPE cells that fully covers Bruch's membrane and the choriocapillaris. We refer to this preparation as "RPE-choroid."

Succinate enhances OCR in the RPE-choroid but not in the retina

Once succinate is taken up, succinate dehydrogenase oxidizes it to fumarate, and the electrons are used by complex IV to reduce O_2 to H_2O. *Ex vivo* RPE-choroid depletes $^{13}C_4$-succinate from the culture medium in a concentration-dependent manner (Figure 1A). We used a tissue perifusion apparatus (Neal et al., 2015) to measure the OCR by RPE-choroid. Succinate substantially increases OCR above the baseline respiration with glucose alone (Figure 1B).

To be certain our measures of succinate uptake and OCR are comparable, we predicted OCR from succinate uptake then compared predicted and experimental values. We used two prediction models, based either on the stoichiometry of electron donation from succinate to O_2 (electrons from two succinate molecules are needed to reduce one O_2 molecule, e.g.,

divide succinate import rate by two) or complete succinate oxidation in the tricarboxylic acid (TCA) cycle (complete oxidation of one succinate molecule results in reduction of three O_2 molecules, e.g., multiply import rate by three). At all concentrations of succinate we tested, experimental OCR fell between the predictions of the two models, suggesting that our experimental systems are well aligned and that succinate uptake does not result in complete oxidation to CO_2 (Figure 1C). We also confirmed that succinate uptake is tissue specific: unlike OCR by RPE-choroid, retina OCR is affected only slightly even by 100 mM succinate (Figure 1D). These results confirm our previous finding that RPE-choroid consumes succinate faster than retinas (Bisbach et al., 2020).

The effect of succinate on OCR in RPE-choroid could reflect its use as a mitochondrial fuel or alternatively as a stimulator of the G-protein-coupled receptor SUCNR1. The EC_{50} of SUCNR1 for succinate 4.5–56 μM (Geubelle et al., 2017; He et al., 2004), and we use far higher concentrations of extracellular succinate in our experiments. However, SUCNR1 also is unlikely to stimulate OCR in the RPE-choroid because 500 μM of the agonist *cis*-epoxysuccinate (EC_{50}: 2.7 μM) does not alter OCR (Figure S1).

Do RPE-choroid cells need to be leaky to consume succinate?

Our findings suggest that rapid consumption of succinate is a biological activity of cells in the RPE-choroid. However, an alternative explanation is that succinate is consumed by mitochondria only in cells damaged during tissue isolation, as has been suggested for liver, heart, and fibroblasts (Jolly et al., 1979; Mapes and Harris, 1975). To distinguish these explanations, we used the following strategies to estimate plasma membrane damage and evaluate its influence on succinate consumption:

    1.   Quantify ^{14}C-sucrose that can infiltrate tissue.

Water enters all cells, but there are no sucrose transporters in mice. Intact cells take up ^3H_2O, but exclude ^{14}C-sucrose, whereas leaky cells should take up both ^3H and ^{14}C. We incubated freshly prepared mouse retinas and RPE-choroid with ^3H_2O and ^{14}C-sucrose for 1 h and quantified tissue ^3H and ^{14}C uptake as a percentage of total for each radioactive dose. Retinas retained 0.34% of the total ^3H_2O dose and 0.09% of the total ^{14}C-sucrose dose. RPE-choroid retained 0.17% of the total ^3H_2O dose and 0.05% of total ^{14}C-sucrose. The ratios of sucrose uptake to water uptake within each tissue suggests that retinas are at most 25.4% ± 0.9% permeable, and RPE-choroid is at most 28.6% ± 2.3% permeable (mean ± SEM; Figure 2A). These are upper limits because vasculature and other extracellular compartments contribute substantially to sucrose retention.

    2.   Quantify LDH released from broken cells.

When the plasma membrane of a cell is disrupted, intracellular components such as lactate dehydrogenase (LDH) and metabolites diffuse from the cytoplasm into the culture medium (Figure 2B). We measured LDH activity in the media into which the dissected retinas and RPE-choroid had been placed and incubated for 1 h. The media contained 0% of the LDH that was in the retina and <10% of the LDH that was in the RPE-choroid. As a positive control to show that permeabilization releases intracellular components, we measured LDH remaining in the tissues over a range of concentrations of digitonin, a non-ionic detergent

(Figure 2C). We confirmed that release of LDH into the medium reached its maximum level by measuring LDH in aliquots of medium over time (Figure 2D).

3.   Evaluate the effect of permeabilization on import of succinate into RPE-choroid.

The percentage of cells in the mouse retina damaged during dissection is 0%–25% based on our radioisotope and LDH experiments. It is slightly higher in RPE-choroid preparations (10%–30%). Those broken cells could account for succinate usage by RPE-choroid, and the intact cells would not contribute at all to succinate uptake. If that hypothesis were correct, adding digitonin to permeabilize the remaining cells that had been intact would allow more succinate to access their mitochondria. Succinate depletion would increase substantially. We tested this hypothesis by incubating retinas and RPE-choroid with 5 mM glucose, 50 μM $^{13}C_4$-succinate, and increasing amounts of digitonin (Figures 2E-2H). We used gas chromatography-mass spectrometry (GC-MS) to quantify metabolites in the tissue and media.

Digitonin decreases export of glycolytic end products lactate and pyruvate by RPE-choroid and retina. This is consistent with permeabilization disrupting glycolysis by allowing diffusion of glycolytic metabolites and enzymes out of the tissue (Figures 2E and 2G). Digitonin does not increase the rate of $^{13}C_4$-succinate depletion by RPE-choroid tissue (Figure 2F). That shows that even in the absence of digitonin, all cells in the RPE-choroid, not just broken cells, import succinate. In retinas, digitonin substantially increased the rate of $^{13}C_4$-succinate depletion, indicating that unlike in the RPE-choroid, succinate is not transported into the retina until cells are permeabilized (Figure 2H).

Unique features of succinate as a fuel for RPE-choroid mitochondria

O$_2$ consumption stimulated by succinate is uniquely rapid—In mitochondria, succinate is oxidized at the inner surface of the inner mitochondrial membrane by complex II (succinate dehydrogenase), which delivers electrons directly into the electron transport chain (ETC). Other fuels (e.g., pyruvate, lactate, glutamine) are oxidized in a qualitatively different way, by soluble enzymes either in the cytoplasm or in the mitochondrial matrix that deliver reducing power to the ETC via NADH and complex I. Those fuels are not as effective as succinate at stimulating O$_2$ consumption by RPE-choroid preparations (Bisbach et al., 2020).

To determine how succinate can be so effective at stimulating OCR, we analyzed metabolic flux using either 1 mM $^{13}C_4$-succinate as a fuel or 1 mM pyruvate + 1 mM $^{13}C_4$-malate. Malate and pyruvate are commonly used together to fuel respiration in isolated mitochondria (Doerrier et al., 2018). Pyruvate provides 2 carbons to make acetyl-CoA, and malate provides 4 carbons to make oxaloacetate. In the canonical TCA cycle, both reactions produce NADH, and the products can be condensed to make citrate. We quantified OCR by the RPE-choroid as a function of concentration of these substrates. Succinate stimulates much more O$_2$ consumption than pyruvate/malate (Figure 3A).

This difference in OCR could result from succinate uptake that is more rapid than pyruvate or malate uptake. To determine if this occurs, we measured the rate at which RPE-choroid depletes each metabolite from culture medium (Krebs-Ringer bicarbonate buffer [KRB]

containing 5 mM glucose, 1 mM pyruvate, 1 mM malate, and 1 mM succinate). Eyecups consume pyruvate and malate at least as fast as succinate, suggesting that OCR from succinate is not greater due to faster uptake (Figure 3B).

In RPE-choroid, neither succinate nor malate are oxidized fully by the TCA cycle, but partial succinate oxidation fuels OCR

We investigated the metabolic basis for this difference by comparing flux from succinate and flux from pyruvate/malate. We incubated freshly dissected RPE-choroid with medium containing 5 mM glucose and either 1 mM of $^{13}C_4$-malate (with 1 mM ^{12}C-pyruvate) or 1 mM $^{13}C_4$-succinate. After 10 min, we collected tissues and media to quantify ^{13}C labeling in metabolites. Individual metabolites establish distinct distributions between the tissue and medium (Figure S2). This is further evidence that plasma membranes in the RPE-choroid preparation are intact and function as a selective barrier.

Figure 3C shows the canonical TCA cycle and the pathways for these labeled substrates. Figures 3D and 3E show accumulation of labeled intermediates in the tissue (black) and in the medium (blue) at 10 min. When the labeled substrate is $^{13}C_4$-malate, 44.1% ± 3.8% of the downstream ^{13}C label in RPE-choroid tissue is on m+4 fumarate, which is predominantly exported. Only a small portion of labeled malate is converted to downstream metabolites, showing that export of malate is much faster than oxidation of malate to oxaloacetate. The TCA cycle intermediate amounts and isotopologue distributions are available as Figure S3.

$^{13}C_4$-succinate that enters mitochondria can be oxidized to fumarate then hydrated to malate. At 10 min, 17.2% ± 0.8% of the ^{13}C label downstream of succinate in RPE-choroid tissue is m+4 fumarate, and 52.0% ± 4.1% is m+4 malate. The majority of fumarate and malate is exported. If we assume linear fumarate and malate generation over time in this experiment, these metabolites are synthesized at 221 ± 44 pmol/min/RPE-choroid (Figure 3E). This is more than half the $^{13}C_4$-succinate uptake rate (Figure 1A) and is thus the dominant form of succinate metabolism under these conditions. Like the incubation in $^{13}C_4$-malate, only limited amounts of metabolites downstream of oxaloacetate had ^{13}C in them (Figure 3E).

When either ^{13}C label enters mitochondria and is oxidized, the total labeled carbon downstream of oxaloacetate is similar, but OCR is stimulated by succinate much more than by pyruvate and malate (Figures 3A, 3C, and 3D). To better account for differences in OCR, we quantify "energetically productive" carbon that by 10 min participated in oxidative reactions. We integrated TCA cycle intermediates metabolized either from $^{13}C_4$-succinate or from $^{13}C_4$-malate. We excluded a metabolite if it was in the medium from the start (e.g., m+4 succinate in $^{13}C_4$-succinate-incubated samples) or if it was not energetically productive (m+4 fumarate from m+4 malate). Oxidation of $^{13}C_4$-succinate and export of its products stimulates substantial consumption of O_2 (Figure 3F). These reactions account for 69% of ^{13}C from $^{13}C_4$-succinate uptake (293 of 422 pmol/min/RPE-choroid). In contrast, import of $^{13}C_4$-malate does not contribute to oxidation reactions, and flow of its carbons to downstream TCA intermediates is slow.

In summary, the mouse RPE-choroid preparation rapidly oxidizes $^{13}C_4$ succinate (Figure 3A) and exports the products (Figure 3E). In contrast, when pyruvate and malate are used as fuel, there is comparably little oxidation of $^{13}C_4$ malate prior to the metabolites produced from it getting exported (Figure 3D).

Uncoupling by succinate

Respiration in most cells is coupled to ATP synthesis by the proton-motive force ($\Delta\rho$). A high $\Delta\rho$ is a thermodynamic barrier to H^+ translocation by complexes I, III, and IV. Flow of protons to the matrix that is not through ATP synthase can uncouple electron transport from ATP synthesis. Uncoupling allows unrestrained electron transport to reduce O_2 to H_2O. We hypothesized that the high rate of OCR when RPE-choroid oxidizes succinate could be caused by uncoupling. We tested this by initially fueling RPE-choroid O_2 consumption with glucose (Figure 4A). Addition of the ATP synthase inhibitor oligomycin almost completely inhibited transport of electrons to O_2, indicating that mitochondria in the tissue were tightly coupled. Oligomycin was present throughout the rest of the experiment. Remarkably, addition of 5 mM succinate (at 90 min) overcame the inhibition and stimulated O_2 consumption to ~3-fold its original rate. Therefore succinate not only provides electrons to reduce O_2 but also uncouples respiration from ATP synthesis. Succinate has these effects over a broad range of concentrations (Figure 4B). Pyruvate and malate are less effective than succinate at overcoming the effect of oligomycin but still stimulate a mild oligomycin-insensitive OCR (Figure 4A). This suggests that oligomycin-insensitive OCR could depend on the rate of substrate oxidation, which for succinate is more rapid.

If succinate uncouples mitochondria by dissipating $\Delta\rho$, it would enhance electron transport at both complex I and complex II. Figure 4C confirms that oligomycin fully inhibits O_2 consumption fueled only with glucose. Addition of succinate increases OCR substantially even in the continued presence of oligomycin. To determine if all the additional OCR is from oxidation of succinate or from oxidation of NADH at complex I, we added rotenone, a selective complex I inhibitor. Blocking complex I partially inhibits succinate-stimulated OCR (by ~0.2 nmol O_2/min/RPE-choroid). The portion of succinate-stimulated OCR blocked by rotenone is from transport of electrons from NADH through complexes I, III, and IV to O_2, as it is inhibited entirely either by antimycin A or by potassium cyanide (Figures 4G and 4J). That rules out superoxide formation through reverse electron transport at complex I as a source of rotenone-sensitive OCR (Robb et al., 2018).

In brown adipose cells and tissue, succinate stimulates production of ROS that causes uncoupling through the actions of an uncoupling protein (Echtay et al., 2002; Mills et al., 2018). We asked whether succinate stimulates the formation of reactive oxygen species (ROS), and whether mitochondrial ROS impacts succinate-stimulated respiration in RPE-choroid. We measured the production of H_2O_2 in culture medium using extracellular HRP and Amplex Red (Figures 4D and 4E) and the ratio of reduced to oxidized glutathione (GSH/GSSG) (Figure 4F). Neither of these measures changes with addition of succinate, though antimycin A treatment decreases the GSH/GSSG ratio.

Mitochondrial ROS are generated at sites I_Q or III_Q in the ETC (Wong et al., 2019; Wong et al., 2017). ROS generation at these sites is inhibited by SI_QEL or $SIII_QEL$ (Goncalves

et al., 2020). Neither suppresses succinate-dependent oligomycin-insensitive respiration by RPE-choroid (Figure S5A). Similarly, the antioxidants mitoTempo (50 μM) or n-propyl gallate (100 μM) do not affect the ability of succinate to overcome the inhibitory effect of oligomycin (Figures S5B and S5C), suggesting that ROS do not drive the uncoupling caused by succinate in RPE-choroid.

Another source of uncoupling could be formation of a mitochondrial permeability transition pore complex (mPTP) (Novgorodovsot et al., 1992). The mPTP is a large unselective channel permeable to multiple ionic species and larger molecules. It is stimulated by high mitochondrial Ca^{2+} and inhibited by cyclosporine A. If succinate drives formation of the mPTP, it could increase respiration. Cyclosporine A does not influence succinate-stimulated OCR (Figure 4G). Furthermore, the mPTP should not form in the absence of Ca^{2+}. For the experiments shown in Figure 4H, we used the Ca^{2+} chelator EGTA (8.6 mM) throughout the tissue dissection and the OCR experiment, yet it did not prevent oligomycin-resistant succinate-stimulated respiration.

Succinate uncouples intact mitochondria in the RPE-choroid

Succinate-dependent uncoupling of electron transport from ATP synthesis could occur for one of two reasons: (1) succinate directly uncouples intact mitochondria, or (2) in RPE-choroid there is a subpopulation of "non-intact" mitochondria, perhaps destined for autophagy, that can perform electron transport but not generate ATP due to a leaky inner mitochondrial membrane. To evaluate the effect of succinate on intact mitochondria, we used mitochondria isolated from mouse brains. The respiratory control ratio (RCR) is a measure of mitochondrial membrane intactness. It is the ratio of respiration with ADP over respiration when ATP synthase is inoperative (with oligomycin). Using pyruvate and malate as fuel, RCR is >5.5, indicating that the mitochondria are intact, and respiration is well coupled (Figure 4I, inset). Following inhibition of ATP synthase with oligomycin (state 4_O respiration), we added increasing concentrations of succinate and measured O_2 consumption. Even in the presence of oligomycin, succinate stimulates respiration by these intact mitochondria to a level approaching state 3 values (Figure 4I). We next asked if the ability of succinate to uncouple mitochondria is complete, like with the classical uncoupler FCCP (carbonyl cyanide p-trifluoro methoxyphenylhydrazone). We measured OCR in intact RPE-choroid with increasing concentrations of succinate to maximally stimulate respiration. FCCP increases respiration above the maximal level achieved by succinate, suggesting that succinate only partially uncouples mitochondria (Figure 4J). An important caveat to this interpretation is that the RPE-choroid preparation comprises at least two cell types, a monolayer of RPE cells and choroidal endothelial cells under the RPE. The respiration uncoupled by FCCP could represent a population of mitochondria that is distinct from those that are uncoupled by succinate. Consistent with the interpretation that succinate uncouples mitochondria is the finding that succinate does not stimulate an increase in ATP levels or ATP/ADP (Figures S6A and S6B). A notable limitation of this interpretation is the possibility that the same data would be produced if succinate increased the rate of both ATP production and consumption. Future experiments using $H_2{}^{18}O$ to estimate ATP flux (Dawis et al., 1989) with or without succinate may resolve this issue.

DISCUSSION

Our study reveals two important concepts about energy metabolism in the vertebrate eye.

1. 70%–90% of cells are intact in dissected RPE-choroid. These intact cells are responsible for succinate import and oxidation.

We show this by quantifying OCR, $^{13}C_4$-succinate depletion and oxidation of $^{13}C_4$-succinate to downstream metabolites. Our findings in RPE-choroid are consistent with reports that succinate stimulates consumption of O_2 by explants of dog heart and by rabbit kidney (Furchgott and Shorr, 1948).

In striking contrast to RPE-choroid, retinas resist succinate import and succinate-stimulated O_2 consumption. We detect succinate uptake by the retina only when it is permeabilized with digitonin. Our retina findings are similar to reports that succinate does not stimulate metabolism in isolated platelets or islets (MacDonald et al., 1989; Ehinger et al., 2016), and that, like liver cells (Mapes and Harris, 1975), retinas metabolize succinate only when damaged or permeabilized.

The general conclusion from our findings is that succinate is cell impermeant only to some types of cells and that cell-type-specific import and export mechanisms dictate which tissues are affected by succinate.

2. Electron transport to O_2 in RPE-choroid mitochondria resists inhibition by oligomycin when succinate is a metabolic substrate.

Exogenous succinate can uncouple ATP synthesis from electron transport either from complex II or from NADH that enters the ETC via complex I. Our controls suggest that oxidation of succinate is not associated with mitochondria disrupted by oxidative stress, the mPTP, or in disrupted mitochondrial membranes. We directly and rigorously show that these factors are not responsible for succinate-stimulated uncoupling. Our findings indicate that oxidation of succinate and succinate-stimulated uncoupling occur in intact cells in our preparations.

How does succinate uncouple mitochondria?

Succinate oxidation can stimulate a high ρ (Mookerjee et al., 2021). There is an exponential relationship between ρ and H^+ leak (Nicholls, 1974, 1997). The current best explanation that we know of is that high ρ causes dielectric breakdown of the mitochondrial membrane (Nicholls, 1974). This is consistent with our findings but we cannot prove it. RPE cells are pigmented, so they are inaccessible to the fluorometric methods used to determine mitochondrial membrane potential. We cannot determine within a single mitochondrion both membrane potential and OCR simultaneously, which could test this hypothesis. Follow-up investigations should focus on determining if dielectric breakdown is responsible for uncoupling respiration from ATP synthesis in RPE/choroid. An alternate hypothesis that also should be tested is that there may be distinct mitochondrial populations in the RPE-choroid, which could include non-intact mitochondria or mitochondria in a different cell type.

In a previous study, we established the possibility that RPE-choroid may oxidize succinate from the retina (Bisbach et al., 2020). Our new data add more support to the model of succinate and malate exchange that we proposed occurs between retina and RPE. We add to this model the idea that when the retina releases succinate, O_2 consumption by the RPE may become uncoupled from ATP synthesis. If that occurs, it could contribute to the remarkably low O_2 pressure in regions of the retina near the RPE. Low retinal O_2 pressure is generally thought to be a consequence of high OCR by the retina, but our findings suggest that comparable or even greater OCR in the succinate-stimulated RPE-choroid also depletes O_2. Low O_2 pressure in the retina, possibly maintained by succinate, may help protect it from light-induced oxidative damage.

Limitations of the study

We identify three critical limitations that should impact the interpretation of this study. The first is that we do not have information about the actual extracellular succinate levels in the small extracellular space between the retina and RPE in intact eyes *in vivo*. Secondly, our experiments were performed *ex vivo*, and we do not know the extent to which O_2 consumption by *in vivo* RPE-choroid is succinate dependent. Finally, we do not have information about the role of this system in sustaining retina or RPE physiology *in vivo*. Our future studies will address these current limitations.

STAR★METHODS

RESOURCE AVAILABILITY

Lead contact—Further information and requests for data, resources and reagents should be directed to and will be fulfilled by the lead contact, James Bryant Hurley (jbhhh@uw.edu).

Materials availability—This study did not generate new unique reagents.

Data and code availability

- Data generated in this study is available upon request.

- This paper does not report original code.

- Any additional information required to reanalyze the data reported in this work paper is available from the lead contact upon request

EXPERIMENTAL MODEL AND SUBJECT DETAILS

Ethical approval—This study was carried out in accordance with the National Research Council's Guide for the Care and Use of Laboratory Animals (*8th ed*). All protocols were approved by the Institutional Animal Care and Use Committees at the University of Washington.

Animals—All experiments used 2–5 month-old male and female wild-type C57BL6/J mice (RRID: IMSR_JAX:000664). These mice were group housed at an ambient temperature of

25°C, with a 12-hour light cycle and *ad libitum* access to water and normal rodent chow. Animals were allocated to study groups randomly.

In all *ex vivo* labeling experiments, we quickly euthanized mice by awake cervical dislocation, enucleated the eye, and trimmed away extraocular muscles. In Hank's Buffered Salt Solution (HBSS; GIBCO, Cat#: 14025-076) we removed the anterior part of the eye by cutting at the ora serrata, and removed the lens. The remaining retina and RPE-choroid separate with minimal manipulation and were used in different downstream experiments. The outer surface of this RPE-choroid preparation is made of sclera, which is not metabolically active. The inner surface is a monolayer of metabolically active RPE cells that fully covers Bruch's membrane and the choriocapillaris.

METHOD DETAILS

***Ex vivo* metabolic *flux*—**Indicated tissues were incubated in pH 7.4 Krebs-Ringer bicarbonate (KRB) buffer (98.5 mM NaCl, 4.9 mM KCl, 1.2 mM KH_2PO_4 1.2 mM $MgSO_4$-$7H_2O$, 20 mM HEPES, 2.6 mM $CaCl_2$-$2H_2O$, 25.9 mM $NaHCO_3$) supplemented with 5 mM glucose and either 50 μM [U-$^{13}C_4$]-succinic acid (Cambridge isotope CLM-1571), 1 mM [U-$^{13}C_4$]-succinic acid, or 1 mM [U-$^{13}C_4$]-malic acid (CLM-8065) and 1 mM Na Pyruvate. This buffer was pre-equilibrated at 37°C, 21% O_2, and 5% CO_2 prior to incubations. We incubated freshly dissected retinas in 200 μL media and RPE-choroid s in 100 μL, all at 37°C, 21% O_2, and 5% CO_2. To determine metabolite uptake or export rate we samples incubation media before (0 minutes), 20 minutes, or 40/45 minutes after the beginning of the incubation. Following incubations, media samples and tissue were flash frozen in liquid N_2. To compare flux of U-$^{13}C_4$-succinate with flux of U-$^{13}C_4$-malate/ unlabeled pyruvate, we incubated RPE-choroid tissue for 10 minutes at 37°C, 21% O_2, and 5% CO_2 before flash freezing tissue and media samples in liquid N_2.

Metabolite extraction—Metabolites were extracted using 80% MeOH, 20% H_2O supplemented with 10 μM methylsuccinate (Sigma, M81209) as an internal standard to adjust for metabolite loss during the extraction and derivatization procedures. The extraction buffer was equilibrated on dry ice, and 150 μL was added to each sample. Tissues were then disrupted by sonication and incubated on dry ice for 45 minutes to precipitate protein. Proteins were pelleted at 17,000 × g for 30 minutes at 4°C. The supernatant containing metabolites was lyophilized at room temperature until dry and stored at −80°C until derivatization. The pellet containing protein was resuspended by sonication in RIPA buffer (150 mM NaCl, 1.0% Triton X-100, 0.5% sodium deoxycholate, 0.1% SDS, 50 mM Tris, pH 8.0) and protein was determined by a BCA assay (ThermoFisher, 23225).

Metabolite derivatization—Lyophilized samples were derivatized with 10 μL of 20 mg/mL methoxyamine HCl (Sigma, Cat#: 226904) dissolved in pyridine (Sigma, Cat#: 270970) and incubated at 37°C for 90 minutes. Samples were further derivatized with 10 μL tert-butyldimethylsilyl-N-methyltrifluoroacetamide (Sigma, 394882) and incubating at 70°C for 60 minutes.

Gas chromatography-mass spectrometry—Metabolites were analyzed on an Agilent 7890/5975C GC-MS using methods described extensively in previous work (Du et al., 2015). Briefly, One microliter of derivatized sample is injected and delivered to an Agilent HP-5MS column by helium gas (flow rate: 1 mL/min). The temperature gradient starts at 100°C for 4 minutes then increases by 5°C/min to 300°C, where it is held for 5 min. We collect masses after a 6.5-min solvent delay. Select ion monitoring (SIM) records only selected m/z in expected retention time windows. These masses range from m/z: ~50–600. Retention times are validated using a solution consisting of known concentrations of specific metabolites we observe it tissue.

Peaks were integrated in MSD ChemStation (Agilent), and correction for natural isotope abundance was performed using the software IsoCor (Millard et al., 2012). Corrected metabolite signals were converted to molar amounts by comparing metabolite peak abundances in samples with those in a 'standard mix' containing known quantities of metabolites we routinely measure. Multiple concentrations of this mix were extracted, derivatized, and run alongside samples in each experiment. These known metabolite concentrations were used to generate a standard curve that allowed for metabolite quantification. Metabolite abundance was normalized to tissue protein concentration, and following this, paired tissues such as retinas and RPE-choroid from the same mouse were treated as technical replicates and averaged.

***Ex vivo* oxygen consumption—**Following euthanasia, mouse tissues were dissected and cut into quarters in Hank's buffered salt solution. These tissues were incubated in Krebs-Ringer bicarbonate buffer (KRB) supplemented with 5 mM glucose and pre-equilibrated at 37°C and 5% CO_2. We determined OCR using a custom-built perifusion flow-culture system (Neal et al., 2015). Tissues were perifused in chambers between Cytopore beads (Amersham Biosciences, Piscatawy, NJ) and porous frits. With KRB supplemented with 5 mM glucose, $1 \times$ Antibiotic-Antimycotic (Gibco), and 1 mg/mL fatty acid-free bovine serum albumin. An artificial lung oxygenated supplemented KRB with a mixture of 21% O_2, 5% CO_2, and 74% N_2. Oxygenated media was passed through a bubble trap before exposure to mouse tissues. Outflow media came into contact with a glass wall coated with a thin layer of oxygen sensitive polymerized Pt(II) Meso-tetra(pentafluorophenyl)porphine dye (PtT975, Frontier Scientific, Logan, UT) painted on the inner glass wall of the chamber. Following a 405 nm light pulse, the dye-coated glass emits a phosphorescent signal detected at 650 nm. The decay lifetime is dependent on oxygen tension. The flow rate of KRB along with the quantitative relationship between dye phosphorescent decay and oxygen concentration were used to determine tissue OCR. All OCR measurements were obtained under control conditions (baseline, 5 mM glucose), one or more experimental conditions, and a 'zeroed' condition wherein 3 mM potassium cyanide (KCN) was used to directly inhibit complex IV and thus subtract the effect of residual non-mitochondrial oxygen consumption from our measurements.

Lactate dehydrogenase assays—We quantified LDH levels using a CyQuant™ Cytotoxicity Assay kit (ThermoFisher C20300) and followed the manufacturers protocol. To obtain samples we dissected retinas and RPE-choroid s, incubated them in 200 μL (retina)

or 100 μL (RPE-choroid) KRB buffer, supplemented with 5 mM ^{12}C-glucose and 50 μM ^{13}C-succinate and indicated concentrations of digitonin. We sampled 5 μL of incubation media at the indicated times for analysis. At the end of the experiment we homogenized tissue in 200 μL of lysis buffer (10% Triton X-100) and 5 μL was used for tissue LDH quantification. We confirmed that all absorbance (490 nm) measurements were in the linear range of the reaction using a BioTek Synergy 4 plate reader.

Measurement of H$_2$O$_2$—Freshly dissected RPE-choroid was incubated for 3 hours in 200 μL KRB with 5 mM glucose, 5 U/mL HRP, 25 U/mL SOD1, and 25 μM amplex red reagent (Thermo-Fisher). H$_2$O$_2$ is produced in cells and diffuses through the plasma membrane. Extracellular H$_2$O$_2$ is used by HRP to oxidize Amplex Red to resorufin. We measured resorufin fluorescence (ex: 550 nm, em: 585 nm) in 10 μL media samples from samples and tissue free control aliquots using a Biotek Synergy 4 plate reader. H$_2$O$_2$ concentration was then quantified using a standard curve of known H$_2$O$_2$ concentrations.

Measurement of GSH and GSSG levels—Freshly dissected RPE-choroid was incubated for 60 minutes in 1 mL of KRB + 5 mM glucose, KRB + 5 mM glucose + 5 mM succinate, or KRB + 5 mM succinate + 10 μM antimycin A. All media was made and equilibrated at 37°C and 5% CO$_2$ prior to the start of the experiment. Following the incubation, tissue was homogenized by sonication in KRB + 2 mM EGTA (250 μL/ sample), and immediately pelleted at 17,000 x g, 4°C, 30 minutes. GSH content was analyzed in duplicate 50 μL aliquots of supernatant using the luciferase-based GSH-Glo glutathione assay (Promega, V6911) following manufacturer's instructions. GSSG + GSH was determined by adding reducing agent tris(2-carboxyethyl)phosphine to the reaction mix (1 mM final concentration). Luminescence was integrated over 1 second and measured on a BioTek Synergy 4 plate reader.

Measurement of ATP and ADP levels—Following a 60 minute incubation in supplemented KRB, RPE-choroid ATP levels were determined by immediately incubating tissue in 100°C Milli-Q H$_2$O for 10 minutes to quench ATPase activity (Yang et al., 2002). Tissue was disrupted by sonication, then insoluble material was pelleted at 17,000 × g and 4°C. ATP and ADP levels were sequentially measured and aqueous supernatant from boiled samples using a luciferin-luciferase based ATP/ADP assay (Sigma, MAK135). Luminescence was measured on a BioTek Synergy 4 plate reader.

Radiation—To measure permeability we compared volume of distribution of an extracellular marker (^{14}C-sucrose) to of ^{3}H$_2$O inside and outside tissue. Uptake of ^{3}H$_2$O and ^{14}C-sucrose (Perkin Elmer, Waltham, MA) was measured as carried out previously (Sweet et al., 2004). ¼ retina or 1 RPE-choroid was incubated in 200 μL KRB with 5 mM bicarbonate in 12 × 75 mm polypropylene test tubes at 37°C for 15 min in a shaking water bath. We added 0.5 mCi ^{3}H and 0.2 mCi for ^{14}C to the tubes and incubated tissue in radiotracer for 60 min. Accumulation of radiolabel was determined by separating the cell-associated radioactivity (CAR) from the free radioactivity by transferring the cell suspension to a 0.4 mL centrifuge tube (USA Scientific, Ocala, FL) with a layer of 1:37.5 n-dodecane:bromo-dodecane (Sigma–Aldrich, St. Louis, MO) and spinning at 12,535 × g,

8 s. The tube was placed briefly in liquid N_2 and we used a razer blade to cut through the radioactive-free oil layer. The bottom portion of the tube containing the tissue was placed into a 7 mL glass scintillation vial. We added 5 mL of Ecolume liquid scintillation cocktail (MP Biomedicals, Cat No. 0188247001) per tube, vortexed the vials, and counted ^3H and ^{14}C using a liquid scintillation counter (Beckman, Model LS6500). The CAR data for each sample was normalized by subtracting the non-specific values and then dividing by the dose. Quench correction for samples was not needed since counts were normalized to the dose and quenching did not vary from sample to sample.

Mitochondrial isolation—Whole mouse brains were dissected into ice-cold mitochondrial isolation buffer (225 mM mannitol, 75 mM sucrose, 1 mM EGTA, 5 mM HEPES, pH 7.0) and homogenized in ice with 5 strokes of a Dounce homogenizer. Homogenate was spun at $1000 \times g$ for 10 minutes to pellet debris and supernatant was transferred to a new tube. Supernatant was spun at $10,000 \times g$ for 10 minutes and supernatant was resuspended in mitochondrial respiration buffer without BSA. We assessed protein concentration using a BCA assay, then performed respirometry using an O2K high-resolution respirometer (Ouroboros). All measurements were performed at steady-state OCR. We stimulated state 3 respiration using sequential additions of pyruvate, malate, and ADP ($\square_F = 0.5$ mM each). We measured state 4_O respiration after adding 10 μM oligomycin, then determined leak respiration using increasing concentrations of succinate ($\square_F = 0.1, 0.3,$ 1, 3, 10 mM). OCR traces were analyzed in DatLab.

QUANTIFICATION AND STATISTICAL ANALYSIS

We performed all statistical data analyses using Prism Version 9 (GraphPad Software). The significance threshold was set at 0.05. To fit curves of oxygen consumption as a function of [succinate], for each sample we averaged steady-state oxygen consumption over >5 minutes at the end of a given treatment. These averaged values were considered as the OCR at each given [succinate] for each sample. We fit the curve to an allosteric sigmoidal shape (Figure 1). We compared flux of ^{13}C (Figure 3) using nonparametric Mann-Whitney tests. Data in all figures are displayed as mean ± SEM. "n" signifies sample size, which is indicated in the figure legend.

Supplementary Material

Refer to Web version on PubMed Central for supplementary material.

ACKNOWLEDGMENTS

REFERENCES

Ast T, and Mootha VK (2019). Oxygen and mammalian cell culture: are we repeating the experiment of Dr. Ox? Nat. Metab 1, 858–860. 10.1038/s42255-019-0105-0. [PubMed: 32694740]

Bisbach CM, Hass DT, Robbings BM, Rountree AM, Sadilek M, Sweet IR, and Hurley JB (2020). Succinate can shuttle reducing power from the hypoxic retina to the O2-rich pigment epithelium. Cell Rep. 31, 107606. 10.1016/j.celrep.2020.107606. [PubMed: 32375026]

Chouchani ET, Pell VR, Gaude E, Aksentijevi D, Sundier SY, Robb EL, Logan A, Nadtochiy SM, Ord ENJ, Smith AC, et al. (2014). Ischaemic accumulation of succinate controls reperfusion injury through mitochondrial ROS. Nature 515, 431–435. 10.1038/nature13909. [PubMed: 25383517]

Dawis SM, Walseth TF, Deeg MA, Heyman RA, Graeff RM, and Goldberg ND (1989). Adenosine triphosphate utilization rates and metabolic pool sizes in intact cells measured by transfer of 18O from water. Biophys. J 55, 79–99. 10.1016/S0006-3495(89)82782-1. [PubMed: 2930826]

Doerrier C, Garcia-Souza LF, Krumschnabel G, Wohlfarter Y, Mészáros AT, and Gnaiger E (2018). High-resolution FluoRespirometry and OXPHOS protocols for human cells, permeabilized fibers from small biopsies of muscle, and isolated mitochondria. Methods Mol. Biol 1782, 31–70. 10.1007/978-1-4939-7831-1_3. [PubMed: 29850993]

Du J, Linton JD, and Hurley JB (2015). Probing metabolism in the intact retina using stable isotope tracers. Methods Enzymol. 561, 149–170. 10.1016/BS.MIE.2015.04.002. [PubMed: 26358904]

Echtay KS, Roussel D, St-Pierre J, Jekabsons MB, Cadenas S, Stuart JA, Harper JA, Roebuck SJ, Morrison A, Pickering S, et al. (2002). Superoxide activates mitochondrial uncoupling protein 2 from the matrix side. J. Biol. Chem 277, 47129–47135. 10.1074/jbc.M208262200. [PubMed: 12372827]

Ehinger JK, Piel S, Ford R, Karlsson M, Sjövall F, Frostner EÅ, Morota S, Taylor RW, Turnbull DM, Cornell C, et al. (2016). Cell-permeable succinate prodrugs bypass mitochondrial complex I deficiency. Nat. Commun 7, 12317–12318. 10.1038/ncomms12317. [PubMed: 27502960]

Furchgott RF, and Shorr E (1948). The effect of succinate on respiration and certain metabolic processes of mammalian tissues at low oxygen tensions in vitro. J. Biol. Chem 175, 201–215. 10.1016/s0021-9258(18)57250-1. [PubMed: 18873295]

Geubelle P, Gilissen J, Dilly S, Poma L, Dupuis N, Laschet C, Abboud D, Inoue A, Jouret F, Pirotte B, and Hanson J (2017). Identification and pharmacological characterization of succinate receptor agonists. Br. J. Pharmacol 174, 796–808. 10.1111/bph.13738. [PubMed: 28160606]

Goncalves RLS, Watson MA, Wong HS, Orr AL, and Brand MD (2020). The use of site-specific suppressors to measure the relative contributions of different mitochondrial sites to skeletal muscle superoxide and hydrogen peroxide production. Redox Biol. 28, 101341. 10.1016/J.REDOX.2019.101341. [PubMed: 31627168]

He W, Miao FJ-P, Lin DC-H, Schwandner RT, Wang Z, Gao J, Chen J-L, Tian H, and Ling L (2004). Citric acid cycle intermediates as ligands for orphan G-protein-coupled receptors. Nature 429, 188–193. 10.1038/nature02488. [PubMed: 15141213]

Hochachka PW, and Dressendorfer RH (1976). Succinate accumulation in man during exercise. Eur. J. Appl. Physiol. Occup. Physiol 35, 235–242. 10.1007/BF00423282. [PubMed: 976251]

Hochachka PW, Owen T, Terrance G, Allen J, Owen JFA, Whittow G, and Causey Whittow G (1975). Multiple end products of anaerobiosis in diving vertebrates. Comp. Biochem. Physiol. B 50, 17–22. 10.1016/0305-0491(75)90292-8. [PubMed: 1122711]

Jang C, Hui S, Zeng X, Cowan AJ, Wang L, Chen L, Morscher RJ, Reyes J, Frezza C, Hwang HY, et al. (2019). Metabolite exchange between mammalian organs quantified in pigs. Cell Metabol. 30, 594–606.e3. 10.1016/j.cmet.2019.06.002.

Jolly WW, Wilhelm DD, and Harris RA (1979). Assessment of tissue and cell damage by succinate oxidation*1. J. Mol. Cell. Cardiol 11, 485–500. 10.1016/0022-2828(79)90472-3. [PubMed: 448744]

Keeley TP, and Mann GE (2019). Defining physiological normoxia for improved translation of cell physiology to animal models and humans. Physiol. Rev 99, 161–234. 10.1152/physrev.00041.2017.-The. [PubMed: 30354965]

Linsenmeier RA, and Zhang HF (2017). Retinal oxygen: from Animals to humans. Prog. Retin. Eye Res 58, 115–151. 10.1016/j.preteyeres.2017.01.003. [PubMed: 28109737]

MacDonald MJ, Fahien LA, Mertz RJ, and Rana RS (1989). Effect of esters of succinic acid and other citric acid cycle intermediates on insulin release and inositol phosphate formation by pancreatic islets. Arch. Biochem. Biophys 269, 400–406. 10.1016/0003-9861(89)90123-9. [PubMed: 2645827]

Mapes JP, and Harris RA (1975). On the oxidation of succinate by parenchymal cells isolated from rat liver. FEBS Lett. 51, 80–83. 10.1016/0014-5793(75)80858-1. [PubMed: 1123069]

Millard P, Letisse F, Letisse F, Sokol S, Sokol S, Portais JC, and Portais JC (2012). IsoCor: correcting MS data in isotope labeling experiments. Bioinformatics 28, 1294–1296. 10.1093/BIOINFORMATICS/BTS127. [PubMed: 22419781]

Mills EL, Cathal Harmon MPJ, Xiao H, Garrity R, Tran NV, Bradshaw GA, Bradshaw GA, Fu A, Szpyt J, Reddy A, et al. (2021). UCP1 governs liver extracellular succinate and inflammatory pathogenesis. Nature Metab. 3, 604–617. 10.1038/s42255-021-00389-5. [PubMed: 34002097]

Mills EL, Pierce KA, Jedrychowski MP, Garrity R, Winther S, Vidoni S, Yoneshiro T, Spinelli JB, Lu GZ, Kazak L, et al. (2018). Accumulation of succinate controls activation of adipose tissue thermogenesis. Nature 560, 102–106. 10.1038/s41586-018-0353-2. [PubMed: 30022159]

Mookerjee SA, Gerencser AA, Watson MA, and Brand MD (2021). Controlled power: how biology manages succinate-driven energy release. Biochem. Soc. Trans 49, 2929–2939. 10.1042/BST20211032. [PubMed: 34882231]

Neal A, Rountree AM, Philips CW, Kavanagh TJ, Williams DP, Newham P, Khalil G, Cook DL, and Sweet IR (2015). Quantification of low-level drug effects using real-time, in vitro measurement of oxygen consumption rate. Toxicol. Sci 148, 594–602. 10.1093/TOXSCI/KFV208. [PubMed: 26396153]

Nicholls DG (1974). The influence of respiration and ATP hydrolysis on the proton-electrochemical gradient across the inner membrane of rat-liver mitochondria as determined by ion distribution. Eur. J. Biochem 50, 305–315. 10.1111/J.1432-1033.1974.TB03899.X. [PubMed: 4452361]

Nicholls DG (1997). The non-ohmic proton leak - 25 Years on. Biosci. Rep 17, 251–257. 10.1023/A:1027376426860. [PubMed: 9337480]

Novgorodovsot SA, Gudz T, I Gudzsqii T, Milgrom Y, M Milgrom Y, Brierley G, and Brierley GP (1992). The permeability transition in heart mitochondria is regulated synergistically by ADP and cyclosporin A. J. Biol. Chem 267, 16274–16282. 10.1016/S0021-9258(18)41996-5. [PubMed: 1644813]

Reddy A, Bozi LHM, Yaghi OK, Mills EL, Xiao H, Nicholson HE, Paschini M, Paulo JA, Garrity R, Laznik-Bogoslavski D, et al. (2020). PH-gated succinate secretion regulates muscle remodeling in response to exercise. Cell 183, 62–75.e17. 10.1016/j.cell.2020.08.039. [PubMed: 32946811]

Robb EL, Hall AR, Tracy A, Prime TA, Szibor M, Eaton S, Szibo M, Viscomi C, James AM, and Murphy MP (2018). Control of mitochondrial superoxide production by reverse electron transport at complex I. J. Biol. Chem 293, 9869–9879. 10.1074/jbc.RA118.003647. [PubMed: 29743240]

Spinelli JB, Rosen PC, Sprenger HG, Puszynska AM, Mann JL, Roessler JM, Cangelosi AL, Henne A, Condon KJ, Zhang T, et al. (2021). Fumarate is a terminal electron acceptor in the mammalian electron transport chain. Science 374, 1227–1237. 10.1126/science.abi7495. [PubMed: 34855504]

Sweet IR, Cook DL, Lernmark Å, Greenbaum CJ, Wallen AR, Marcum ES, Stekhova SA, and Krohn KA (2004). Systematic screening of potential β-cell imaging agents. Biochem. Biophys. Res. Commun 314, 976–983. 10.1016/J.BBRC.2003.12.182. [PubMed: 14751228]

Wong HS, Benoit B, and Brand MD (2019). Mitochondrial and cytosolic sources of hydrogen peroxide in resting C2C12 myoblasts. Free Radic. Biol. Med 130, 140–150. 10.1016/J.FREERADBIOMED.2018.10.448. [PubMed: 30389498]

Wong HS, Dighe PA, Mezera V, Monternier PA, and Brand MD (2017). Production of superoxide and hydrogen peroxide from specific mitochondrial sites under different bioenergetic conditions. J. Biol. Chem 292, 16804–16809. 10.1074/jbc.R117.789271. [PubMed: 28842493]

Yang NC, Ho WM, Chen YH, and Hu ML (2002). A convenient one-step extraction of cellular ATP using boiling water for the luciferin-luciferase assay of ATP. Anal. Biochem 306, 323–327. 10.1006/ABIO.2002.5698. [PubMed: 12123672]

Yu D-Y, and Cringle SJ (2006). Oxygen distribution in the mouse retina. Investig. Ophthalmol. Vis. Sci 47, 1109–1112. 10.1167/IOVS.05-1118. [PubMed: 16505048]

Highlights

- Succinate stimulates mitochondrial respiration in intact RPE-choroid tissue

- Extracellular succinate is imported and oxidized, then exported as fumarate or malate

- Succinate oxidation fuels a higher O_2 consumption rate than NADH-linked substrates

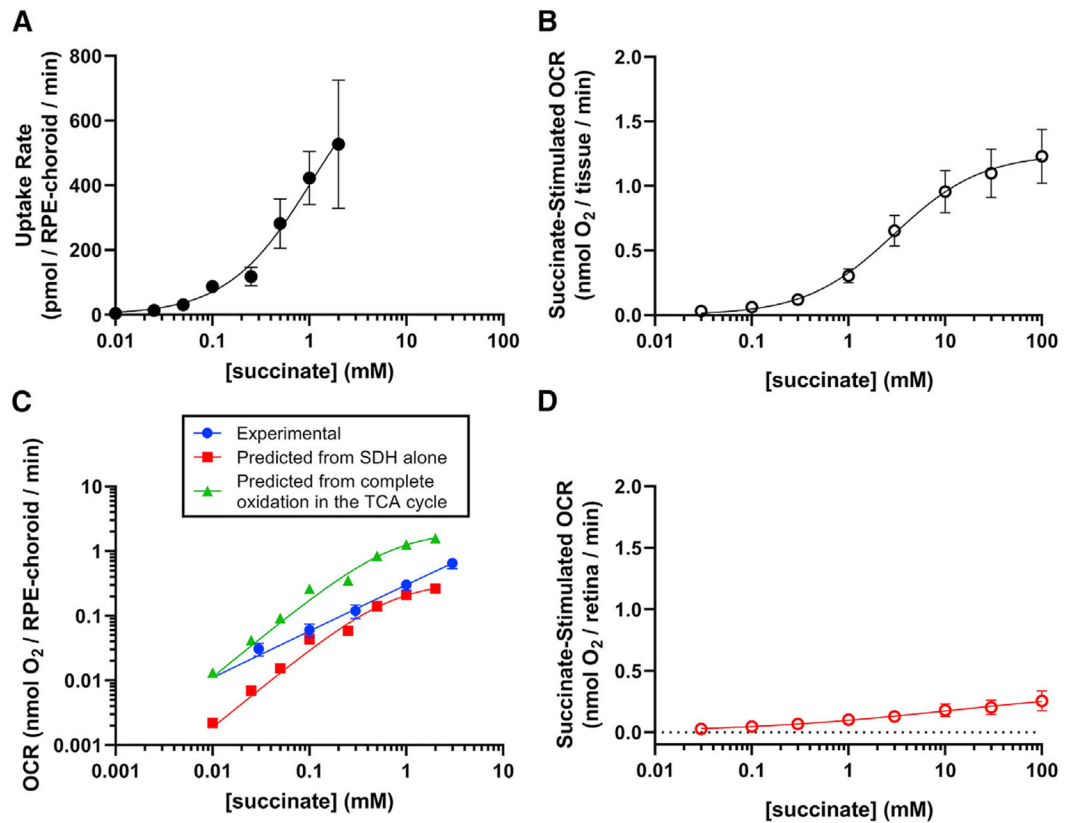- Respiration from succinate is not well-coupled to ATP synthase activity

Figure 1. Extracellular succinate selectively increases oxygen consumption in RPE-choroid
(A) We determined succinate uptake rate by freshly dissected RPE-choroid from medium containing 0, 10 μM, 25 μM, 50 μM, 100 μM, 250 μM, 1 mM, and 2 mM $^{13}C_4$-succinate (n = 3–15 per concentration). Rate was determined from medium m+4 succinate concentrations at 0, 20, and 40 min after the start of the incubation.
(B) We measured O_2 consumption rate (OCR) in freshly dissected RPE-choroid (n = 5). We supplied this media with increasing concentrations of disodium succinate (30 μM, 100 μM, 300 μM, 1 mM, 3 mM, 10 mM, 30 mM, or 100 mM) and determined steady-state OCR above the 5-mM glucose "baseline" respiration.
(C) We compared experimental OCR (blue circles) with "expected" OCR based on succinate uptake and oxidation only by (succinate dehydrogenase) SDH(uptake rate/2, redsquares) orcomplete oxidation (uptake rate × 3, green triangles).
(D) We measured OCR in retina tissue (n = 4) respiring in KRB buffer with 5 mM glucose and the same concentrations of succinate as in (B). Mean basal OCR with 5 mM glucose as the sole substrate is 0.83 ± 0.26 nmol O_2/minute for retinas and 0.47 ± 0.08 nmol O_2/minute for RPE-choroid. We fit an allosteric sigmoidal curve to the data in each panel. Each point represents the mean ± SEM. See also Figure S1.
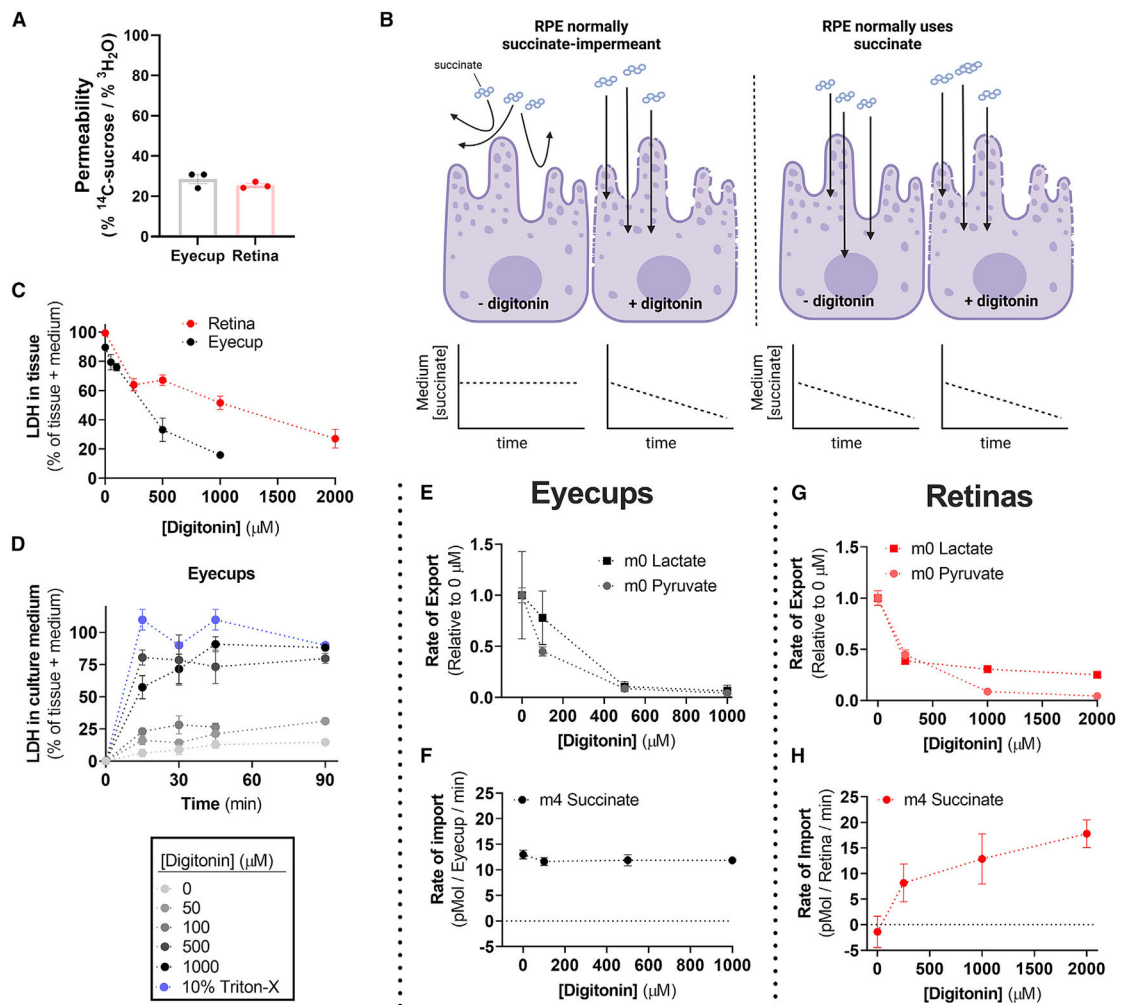
Figure 2. RPE-choroid permeability does not alter succinate uptake or oxidation

(A) Permeability of freshly dissected retina and RPE tissue assessed by the relative uptake of ^3H_2O and ^{14}C-sucrose over an hour *ex vivo* (n = 3).

(B) Model of the hypothesis to test whether succinate oxidation by RPE-choroid tissue is the result of cell permeability.

(C) Retina and RPE-choroid LDH release increases as a function of [digitonin]. Percentage of total was determined by assaying LDH in both tissue and culture medium when [LDH] was at a steady state in medium (n = 2–6 per concentration).

(D) Determination of the *ex vivo* culture time needed to reach steady-state [LDH] (n = 2–4 per concentration).

(E) Relative lactate and pyruvate release rate by RPE-choroid decreases with increasing [digitonin] (n = 8).

(F) RPE-choroid $^{13}C_4$-succinate uptake rate however is unaltered by [digitonin] (n = 8).

(G) As with RPE-choroid tissue, lactate and pyruvate release decreases in retinas with increasing [digitonin] (n = 3–9).

(H) Unlike with RPE-choroid, retina $^{13}C_4$-succinate uptake increases with [digitonin], suggesting that the plasma membrane is a barrier for retina but not RPE-choroid succinate

uptake (n = 3–9). Data are represented as the mean ± SEM. (A) also shows values from individual replicates. See also Figure S2.
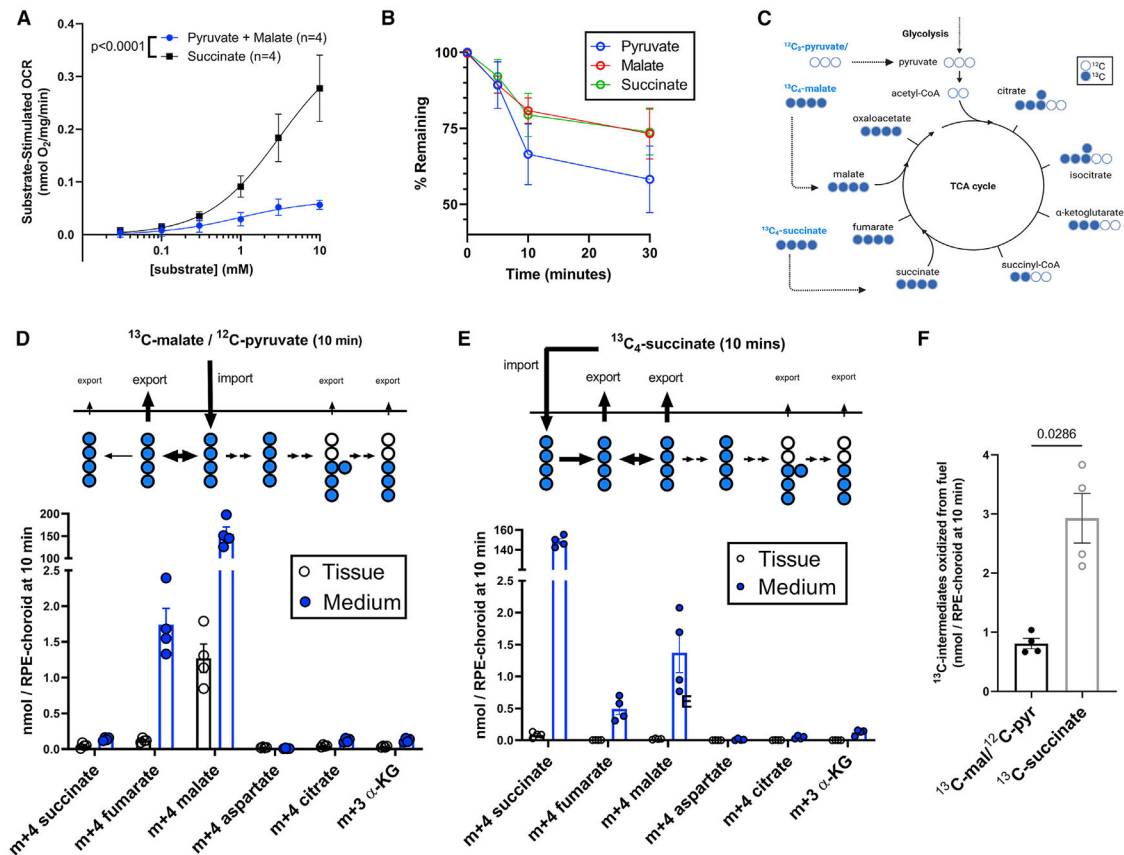
Figure 3. Succinate is preferred over pyruvate/malate for oxidation by RPE-choroid mitochondria

(A) RPE-choroid OCR from 5 mM glucose supplemented with increasing concentrations (30 μM, 100 μM, 300 μM, 1 mM, 3 mM, 10 mM) of succinate or malate and pyruvate (n = 4).

(B) Pyruvate, malate, and succinate uptake (starting concentration: 1 mM ea.) by RPE-choroid *ex vivo*. Media was sampled before tissue was added; then 5, 10, and 30 min later, tissue was added (n = 7–8).

(C) TCA cycle ^{13}C labeling scheme when cells use $^{13}C_4$-malate/^{12}C-pyruvate/^{12}C-glucose or $^{13}C_4$-succinate/^{12}C-glucose as a substrate.

(D) Medium and tissue m+4 succinate, m+4 fumarate, m+4 malate, m+4 aspartate, m+4 citrate, and m+3 α-ketoglutarate in RPE-choroid incubated for 10 min in 1 mM $^{13}C_4$-malate/1 mM ^{12}C-pyruvate/5 mM ^{12}C-glucose (n = 4).

(E) The same metabolites in medium and tissue of RPE-choroid incubated in 1 mM $^{13}C_4$-succinate/5 mM ^{12}C-glucose. In (C)–(D) the metabolite present in incubation medium was excluded from analysis (n = 4).

(F) Quantification of ^{13}C in medium and tissue on energetically useful metabolites from each substrate, using data from (C)–(D). Reported p values result from (A) an extra sum-of-squares F test and (F) two-tailed Mann-Whitney tests. Data are represented as the mean ± SEM, with individual replicates also visible in (D)–(F). See also Figure S3.
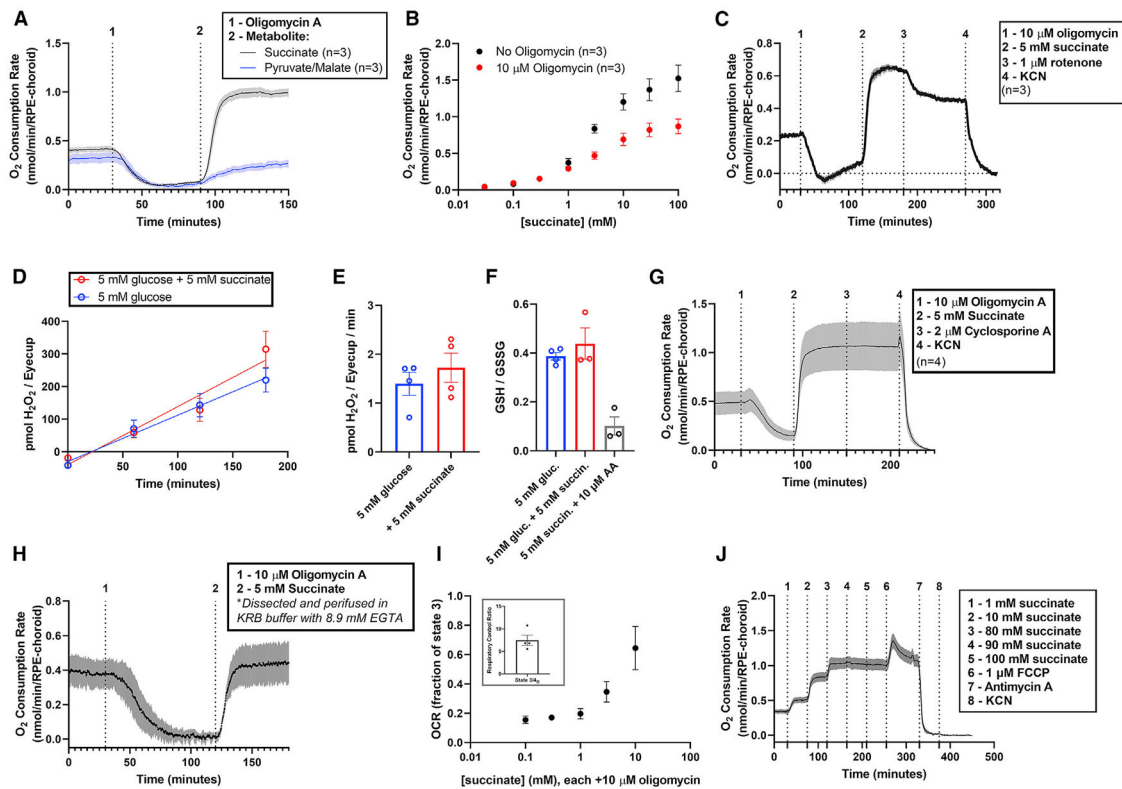
Figure 4. Extracellular succinate is a substrate for and uncoupler of RPE-choroid mitochondria

(A) We determined ATP synthase-independent substrate oxidation by incubating RPE-choroid tissue in 5 mM glucose, then in 5 mM glucose with 10 μM of the ATP synthase inhibitor oligomycin, and finally in a mix of 5 mM glucose, 10 μM oligomycin, and 5 mM of succinate (black) or pyruvate/malate (blue) (n = 3). 10 μM oligomycin is sufficient to maximize its effect on metabolism (Figure S4).

(B) We determined OCR as a function of [succinate] in the presence or absence of 10 μM oligomycin A (n = 3).

(C) To determine whether NADH oxidation was the source of uncoupled respiration, we first stimulated succinate-dependent uncoupling as in (A), then added 1 μM of the complex I inhibitor rotenone (n = 3). This partially inhibited respiration, suggesting that succinate re-actives NADH oxidation after oligomycin shuts it down.

(D–I) We next determined the effect of succinate on the generation of reactive oxygen species by probing (D–E) H_2O_2 generation rate (n = 4) and (F) glutathione redox status (n = 3–4). 5 mM succinate did not alter these parameters, so it is unlikely a source of significant ROS in RPE-choroid. To determine the source of oligomycin-resistant respiration, we performed the treatments described in (A), but following the addition of 5 mM succinate, we attempted to shut down the succinate-dependent increase in OCR by adding (G) the mitochondrial permeability transition pore complex inhibitor cyclosporine A (n = 4) or (H) EGTA to deplete perifusion medium of free Ca^{2+} during the experiment (n = 4). We determined OCR in isolated brain mitochondria using an Oroboros O2K high-resolution respirometer and determined (I, inset) state 3/state 4_O OCR and (I) oligomycin-resistant OCR as a function of [succinate] (from 0.1 to 10 mM; n = 4).

(J) We also determined respiration with saturating concentrations of succinate (80–100 mM) and whether OCR could be increased by addition of FCCP. FCCP does increase respiration, suggesting that in RPE-choroid, succinate is not fully uncoupling all mitochondria (n = 4). Data are represented as mean ± SEM. (E), (F), and the inset of (I) also show values from individual replicates. See also Figures S4-S6.

KEY RESOURCES TABLE

REAGENT or RESOURCE	SOURCE	IDENTIFIER
Chemicals, peptides, and recombinant proteins		
[U-13C]-malate	Cambridge Isotope Labs	Cat# CLM-8065
[U-13C]-succinate	Cambridge Isotope Labs	Cat# CLM-1571
Oligomycin	Caymen Chemical	Cat# 11342
Cyclosporine A	Caymen Chemical	Cat# 12088
S1QEL	Millipore Sigma	Cat# SML1948
S3QEL	Millipore Sigma	Cat# SML1554
n-propyl gallate	Millipore Sigma	Cat# P3130
Mito-tempo	Millipore Sigma	Cat# SML0737
Rotenone	Millipore Sigma	Cat# R8875
Antimycin A	Millipore Sigma	Cat# A8674
Amplex Red	Thermo-Fisher	Cat# A22189
Critical commercial assays		
ATP/ADP Assay	Millipore Sigma	Cat# MAK135
GSH-glo Assay	Promega	Cat# V6911
CyQuant™ Cytotoxicity Assay	Thermo Fisher	Cat# C20300
BCA protein concentration assay	Thermo Fisher	Cat# 23225
Experimental models: Organisms/strains		
C57BL6/J mice	The Jackson Laboratory	RRID: IMSR_JAX:000664
Software and algorithms		
MSD Chemstation E.02.01.1177	Agilent Technologies	https://www.agilent.com/
IsoCor, v1.0	Millard et al., 2012	https://isocor.readthedocs.io/en/latest/index.html#
DatLab V7.3.0.3	Oroboros Instruments	https://www.oroboros.at/
Prism V9.3.1	Graphpad Software	https://www.graphpad.com/; RRID:SCR_002798